2022 IEEE/RSJ International Conference on Intelligent Robots and Systems (IROS)
October 23-27, 2022, Kyoto, Japan

Tactile Perception for Growing Robots via Discrete Curvature Measurements

Micah Bryant[1], Connor Watson[1], Tania K. Morimoto[2]

***Abstract*— Soft, growing robots have the ability to conform to their environment and traverse highly curved paths that would typically prove challenging for other robot designs. As they navigate through these constrained and cluttered environments, there is often significant interaction between the robot and its surroundings. In this work, we propose a method to enable tactile perception for growing robots, which utilizes commercially available, flexible sensors that measure the curvature of the robot shape at multiple locations. Our method consists of both a pouch design to enable seamless integration of the sensors with the material of the growing robot, as well as an algorithm for determining the location of point contacts along the robot body. We validate our proposed approach experimentally using a 3.5 cm robot that can grow to be 53 cm long. We show that we can localize a force applied to various locations along its length with an average error of 3.44 ± 1.38 cm when the robot is unactuated and 4.62 ± 0.95 cm when the robot is actuated. Additionally, we characterize the minimum distance required for our tactile sensing approach to discriminate between two separate contact points along the robot body to be 23.5 cm. Finally, we apply our method to a growing robot exploring an unknown environment and show that we are able to effectively determine when and where the growing robot collides with an unknown obstacle.**

I. Introduction

Everting, or growing, robots are a type of continuum robot that has drawn inspiration from biology. They consist of a thin, flexible, hollow tube that is inverted inside itself from one end. Applying an internal pressure causes this inverted material to be pushed, or everted, out from the tip of the robot into the environment (Fig. 1), resulting in a growing motion that resembles that of a plant [1]. Growing robots are naturally compliant, which allows them to conform to their surroundings and traverse highly curved paths. The unique attributes of these robots have motivated their use in a variety of applications such as search and rescue [2], archaeological exploration [3], marine environment observation [4], and minimally invasive surgery [5].

For these applications, the environments are often constrained or highly cluttered, typically resulting in significant interaction between the robot and its surroundings. It therefore becomes important to take robot-environment interactions into account for modeling [6], planning [7] [8], and control [9]. Often, however, the algorithms developed for these robots make assumptions that limit the types of applications for which they can be used. In particular, most planning algorithms developed to date have assumed that a map of the robot's environment is known a priori in order to compute feasible robot trajectories [7] [8], but this is impractical for situations where the robot is exploring unfamiliar territory. Accordingly, sensors must be integrated with growing robots to allow them to perceive their environments on the fly and enable their use in a wider range of applications.

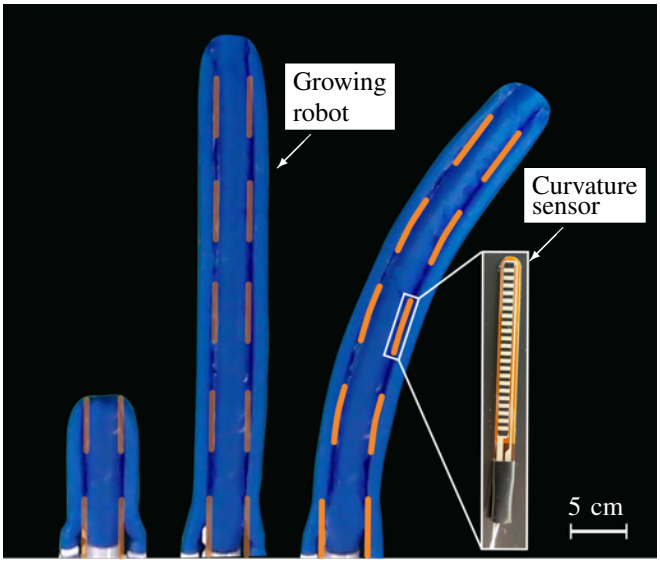

Fig. 1: An actuated growing robot (blue) with integrated curvature sensors (depicted in orange) which we use for tactile perception. From left to right the robot is shown growing and then bending due to applied actuation.

Sensor integration for growing robots can be difficult, however, due to mechanical challenges imposed by the soft, thin-walled body of the robot. Most previous work in this area has centered around methods for the integration of devices at the tip of the robot including cameras [10], magnets [11], and more general payloads [12]. While these approaches provide valuable information at a single point on the robot, growing robots may undergo interactions with the environment anywhere along their length that would be unobservable from a single point measurement. To address this issue, more recent works have looked at distributed sensing methods that can be used to acquire orientation information about the robot, as well as temperature and humidity measurements from the environment, at many points along the length of the robot using flexible bands of sensors [13].

*This work was supported in part by the National Science Foundation under Grant 1935329.

[1]Micah Bryant and Connor Watson are with the Department of Mechanical and Aerospace Engineering, University of California, San Diego, La Jolla, CA 92093 USA. e-mail: mabryant@ucsd.edu (corresponding author).

[2]Tania K. Morimoto is with the Department of Mechanical and Aerospace Engineering and the Department of Surgery, University of California, San Diego, La Jolla, CA 92093 USA.

2022 IEEE/RSJ International Conference on Intelligent Robots and Systems (IROS) | 978-1-6654-7927-1/22/$31.00 ©2022 IEEE | DOI: 10.1109/IROS47612.2022.9981273

In this work, we also adopt a distributed sensing approach to, for the first time, enable tactile sensing for growing robots based on measurements from flexible curvature sensors integrated throughout the robot body. Similar to the work of [14] and [15], wherein the authors estimate loads applied to a flexible rod, our method for estimating contact from curvature relies on adopting a mechanical model of the robot shape, which enables us to interpolate between relatively sparse sensor measurements. Our pursuit of tactile sensing remains bio-inspired — just like the robots themselves — drawing inspiration from vine plants, which depend on a sense of touch to locate support structures on which they can grow [16]. Tactile sensing has the potential to enable growing robots to locate obstacles and support structures, map their environments in real-time, and plan their movement even in previously unexplored environments.

The remainder of the paper is organized as follows. First, we detail the specific hardware used in our growing robot platform and tactile sensing solution. Next, we present an approach for determining point contact locations on the body of our robot from discrete curvature measurements, assuming that the growing robot can be modeled as an inflatable Euler-Bernoulli (EB) beam [17]. Finally, we empirically characterize the performance of our tactile sensing method and conclude with discussions and directions for future work.

II. Robot Hardware

Here we present the design of our growing robot, as well as the method to control its growth and shape.

A. Growing Robot

Our growing robot (Fig. 2) is fabricated using a lightweight, silicone-urethane impregnated ripstop fabric (Seattle Fabrics) that is flexible, but not extensible. The main body of the robot is fabricated by forming this material into an invertible tube using Sil-poxy Silicone adhesive (Smooth-On). The diameter of the robot, when inflated, is 3.5 cm, which was chosen to ensure that the selected sensors, explained in detail in the subsequent section, could be easily everted. The proximal end of the robot body is attached to an inlet of a pressure vessel, whose internal pressure can be controlled to induce robot growth. The distal end of the robot is inverted through the center of the robot and connected using a string to a motorized spool housed inside the pressure vessel. Regulating the position of the spool using an encoder, allows for control of the growth length of the robot, which is 53 cm maximum.

B. Robot Actuators

Two fabric pneumatic artificial muscles (fPAMs) [18] are fabricated with a diameter of 1.6 cm using the same material as the main body. They are attached on opposite sides of the growing robot body using Sil-Poxy Silicone adhesive, such that they can easily evert out with the main body (see Fig. 2). These fPAMs are used to bend, or steer, the robot in the plane, in a manner analogous to tendons. When the pressure inside an fPAM is increased, the fPAM

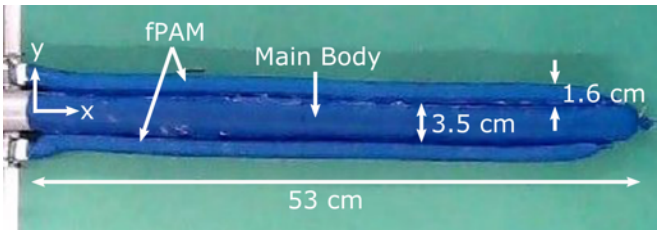

Fig. 2: The fully deployed growing robot, along with critical dimensions for both the main robot body and the fabric pneumatic artificial muscles (fPAMs). The coordinate axes are also defined, where x points in the direction of the straight robot configuration and y is orthogonal to x.

contracts, causing the entire robot to bend. The pressure in each fPAM is controlled by a separate NITRA Current to Pneumatic Transducer (NCP1-20-260N and NCP2-20-260N). The current sent to the regulators is maintained in a pressure feedback loop established using a PID controller and two Honeywell pressure sensors (SSC-series 60 PSI). Both the actuator pressures and the motorized spool position are set by an Arduino Mega 2560, which allows for control of two independent degrees of freedom — the deployed length of the robot and its tip orientation in the plane.

A mapping was created to determine the robot curvature as a function of actuator pressure. This mapping is possible because an fPAM causes approximately constant curvature bending along the entire length of the robot when pressurized [8]. The mapping was created by applying 11 different pressures (0 to 20 psi in 2 psi increments) to each actuator across 3 trials, recording the curvature using an overhead camera, and fitting the data to a hyperbolic tangent function.

III. Sensor Integration

Here we present our sensor choice, integration method, and how we convert the sensor readings into the necessary curvature information.

A. Sensor Selection

Integrating sensors onto the flexible, thin-walled body of a growing robot without adversely affecting the desirable attributes of the robot (e.g. eversion and compliance) is difficult. Many of these challenges stem from the significant stiffness mismatch that typically exists between the sensor materials and robot materials. In addition, the robot can experience uncontrolled wrinkling and the eversion process induces tight curvatures, all of which can lead to significant stress on any integrated sensors. One potential class of sensors that could be used for tactile perception includes flexible pressure sensors. Although these sensors would provide a direct measurement of applied force, they would need to be placed at every point along the robot body in order to generate full robot coverage. Further they would need to be integrated into the outside of the robot body, adding additional fabrication complexity, in order to ensure sufficiently large sensor readings from obstacle contact. We instead find that flexible, resistance-based sensors (Spectra Symbol 2.2")

are an appropriate choice given the design requirements, provided they are properly coupled to the growing robot body. Each sensor is 5.5 cm long and has a resistance proportional to its curvature. Using multiple of these sensors, we can determine local curvature measurements at discrete locations along the growing robot backbone. In order to ensure that the sensor can withstand the bending required for eversion, the base of the sensor is wrapped in tape to strengthen electrical connections with the wires (Fig. 3a).

B. Sensor Integration

Simply adhering the sensors directly to the growing robot is problematic because the robot behaves mechanically as an inflatable beam [17]. Therefore, if stiffer locations exist along the robot body — caused by something such as a flex sensor adhered directly to the robot fabric, for example — the robot will form sharp local kinks around these locations (Fig. 3c) when the robot encounters a contact force, rather than forming a smooth curve [6] [7]. Because such kinks causes a discrete change in the curvature between sensors, it is not measured, making the contact force unobservable.

To solve this issue, we introduce a pouch device (Fig. 3a and Fig. 3b) to house and fasten the curvature sensors to the growing robot. The pouch is made out of the same material as the robot body. It is sewn closed on three sides and is sized such that the sensor can slide inside, while being constrained from unwanted movement (10 cm long, 0.75 cm wide). The pouches are then glued onto the inside body of the robot, using the same Sil-poxy Silicone adhesive, and the sensor is locked in place by gluing another small piece of fabric over the open entrance.

This pouch allows the robot to bend, while avoiding the kinking issue that can be caused by severe stiffness mismatches. Specifically, for a growing robot made from an inextensible material to bend in a given direction, the length of the inner side of the curve must shorten. However, as this material is inextensible, the only way that the fabric can shorten on the inside curve is by uniform wrinkling of the fabric. The pouch enables the sensor to lift slightly off the surface of the robot wall, such that the robot material can wrinkle and the sensor can continue to provide accurate measurements (Fig. 3d). While the pouch and sensor attachment does increase the bending stiffness of the robot, it does not prevent its growing motion. This design makes the combined stiffness of the sensorized robot more uniform and more effectively transmits applied forces to the sensors so that changes in curvature can be measured. For our robot, we place five, 10 cm long pouches into a single column along each side of the robot.

IV. Touch Localization Algorithm

In this section we detail our algorithm for determining the location of point contact forces applied to the body of a growing robot using measurements of the robot's local curvature. Then we discuss details associated with the algorithm's practical implementation.

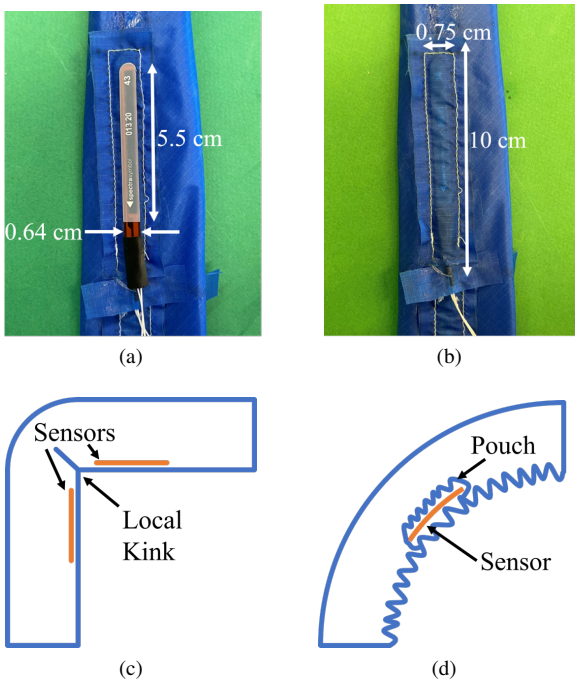

Fig. 3: (a) Example off-the-shelf, flexible sensor used to measure local robot curvature, along with its dimensions. (b) To integrate the sensors with the growing robot, they are sealed inside individual sensor pouches with dimensions as shown. (c) Representation of a sharp local kink that can form in the material due to significant stiffness mismatches if sensors are attached directly. (d) Representation of material wrinkling when sensors are housed inside a custom pouch, resulting in a more uniform stiffness along the robot length.

A. Optimization-Based Localization

We consider a planar robot, which we assume to behave as a cantilever beam and can be described using an EB beam model [17] as

$$EI\frac{d^4y}{dx^4} = q(x), \tag{1}$$

where E is the Young's modulus of the robot, I is it's area moment of inertia, and y is the deflection of the robot due to applied load q at length x. For N_c point contacts, the function describing the applied load is

$$q(x) = \sum_{i=1}^{N_c} F_i\delta(a_i - x), \tag{2}$$

where $\delta(\cdot)$ is the Dirac delta function, F_i is the magnitude of the ith point contact force, and a_i is the contact location along the robot body. The position and orientation of the robot is fixed at its base, which imposes boundary conditions

$$y(x)\Big|_{x=0} = 0, \qquad \frac{dy}{dx}\Big|_{x=0} = 0. \tag{3}$$

As is common for growing robots with pneumatic artificial muscles, we further assume that actuation causes constant

curvature deformation of the robot shape [8], leading to another boundary condition

$$\left.\frac{d^2y}{dx^2}\right|_{x=L} = g(p), \tag{4}$$

which states that the curvature of the robot at the free end is a function of the actuator pressure, $g(p)$. If the robot is unactuated, then $g(0) = 0$. In the case where the robot is actuated, we can empirically fit a function that relates the constant curvature of the robot to the actuator pressure, as described in Section II-B. Integrating Eq. (1) twice with these boundary conditions gives a closed-form expression for the robot curvature,

$$\frac{d^2y}{dx^2} = \hat{k}(x) = g(p) + \sum_{i=1}^{N_c} \frac{F_i}{EI}(a_i - x)H(a_i - x), \tag{5}$$

where $H(\cdot)$ is the Heaviside step function.

In order to determine the location of the point contact forces applied to the robot, we can pose an optimization problem to minimize the difference between the curvature sensor measurements and Eq. (5) at the location of each sensor,

$$\min_{\mathbf{a},\mathbf{f}} \sum_{i=1}^{N_s} ||k_{sensor,i} - \hat{k}(x_i)||_1, \tag{6}$$

where $\mathbf{a} = [a_1, ...a_{N_c}]$ is a vector of point contact locations, $\mathbf{f} = \frac{1}{EI}[F_1, ...F_{N_c}]$ is a vector of the magnitudes of each contact force normalized by the robot bending stiffness, x_i is the position of the ith sensor on the robot body, and $||\cdot||_1$ is the 1-norm. We choose to minimize the 1-norm to mitigate the impact of outliers due to sensor noise [19]. We solve this problem using an interior point method implemented by MATLAB's *fmincon* routine and impose the constraint that $a_i \in [0, L]$. Additionally, we find that solving for both $\mathbf{a}$ and $\mathbf{f}$ simultaneously, typically finds poor locally optimal solutions for the point contact locations, $\mathbf{a}$. Therefore, we iteratively optimize for either $\mathbf{a}$ or $\mathbf{f}$, one at a time, while holding the other constant until the difference between successive solutions for all of the point contact locations is less than a tolerance (0.5 cm). For initialization of each term, we initialize the force terms at 0 and the position terms to be at the tip, since we expect most contact locations to first occur near the tip as the robot grows through an unknown environment. In the case of multiple contacts we split the length into uniform sections for initialization (e.g. for 2 point contacts we initialize the contacts at $\frac{L}{2}$ and L).

B. Implementation Details

As described above, the sensors used in our experiments have a resistance that changes proportionally with their curvature. In order to determine the proportionality constant for each sensor integrated into the robot, we collect resistance measurements from all sensors as the tip of the unactuated robot is deflected to 10 different locations and record the tip positions using an overhead camera. Each of these tip position measurements, y_{tip} is used as a boundary condition,

$$\left.y(x)\right|_{x=L} = y_{tip}, \tag{7}$$

together with the conditions in Eq. (3) and Eq. (4) to solve Eq. (1) for the curvature of the robot at every sensor location. We can then determine the constant relating these curvature values to the collected resistance measurements by computing a linear regression. Once these constants are computed, they can be used to determine the curvature of each sensor from its resistance measurement at any given time.

In addition to using the sensor curvatures to find the location of applied point contacts, we also use the sensor measurements to detect when the robot comes into contact with an unknown force. When the robot is not experiencing a contact force, it should have a constant curvature that depends on its actuator pressure, $g(p)$. If the average curvature measured by the sensors at the base of the robot deviates beyond an empirically determined threshold (0.005 cm^{-1}), then the robot is determined to be in contact with an obstacle and optimization can be used to determine the location of the contact.

V. Experiments and Results

We validate our proposed method for tactile sensing in growing robots through four different experiments. First, we characterize the localization accuracy of our method for a single point contact at different forces and locations on a robot when it is unactuated (i.e. the fPAMs are not actively pressurized). Second, we determine conditions under which our method can discriminate between two contacts on an unactuated robot. Third, we assess contact localization accuracy for an actuated robot. Finally, we demonstrate an application of our method, wherein a growing robot uses our proposed tactile sensing to determine when it is in contact with obstacles as it explores an unknown environment.

A. Experimental Setup

A test environment was fabricated to assess our sensing methodology (Fig. 4). Metal dowels were placed at specified locations in the workspace and served as contacts with which the robot could interact. Their positions, relative to the robot base, were determined from 1920x1080 resolution images taken with an overhead camera (Nexigo N980P). The x and y axes of the coordinate frame of the growing robot are defined as in Fig. 2. In all experiments, localization error is defined as the absolute difference between the x position of the obstacle contact, as estimated by the localization algorithm, and the true obstacle position, as determined by the overhead camera.

B. Single Contact

In this experiment, we look to assess how accurately we can localize an applied force of different magnitudes at various locations along the length of an unactuated robot. Specifically, we consider a low magnitude force and a high magnitude force, each applied to the following three

locations along the robot body: at the tip, $\frac{3}{4}L$, and $\frac{1}{2}L$, where L is the total deployable length of the robot (see Fig. 5a). For this experiment, we apply 0.49 psi to the main body of the robot and collect data (curvature sensor measurements and an overhead camera image) from 5 trials for each of the six loading conditions to determine the repeatability of our results. For each loading condition, Fig. 5c shows the mean error between the position of the contact force on the robot body as determined by our optimization and the position as determined by the overhead camera.

In general, high contact forces result in consistent localization error (3.44 ± 1.38 cm on average, approximately the diameter of the unactuated robot) regardless of the location at which they are applied to the robot (see Fig. 5c). Low magnitude contact forces, on the other hand, tend to result in increasing localization error (4.59 ± 6.78 cm on average) the further away from the tip the force is applied. This difference is likely because lower magnitude forces applied closer to the base of the robot do not induce large changes in the curvature of the robot shape compared to those applied closer to the tip. Smaller changes in robot curvature correspond to smaller magnitude signals from each of the sensor measurements used for optimization, in turn making the optimization more sensitive to sensor noise. As a result, the optimization can end up either over-fitting to noisy readings or failing to move from the initialization point, leading to poor estimates of the contact point location (Fig. 6b). High magnitude forces, however, induce consistently larger changes in robot curvature resulting in more consistent localization regardless of where the force is applied (Fig. 6a). We note that when the high magnitude forces are applied, the sensors at the base have significantly higher curvature measurements relative to the other sensors, which can likely be attributed to the robot buckling at this location. These higher curvature measurements do not, however, significantly impact optimization results.

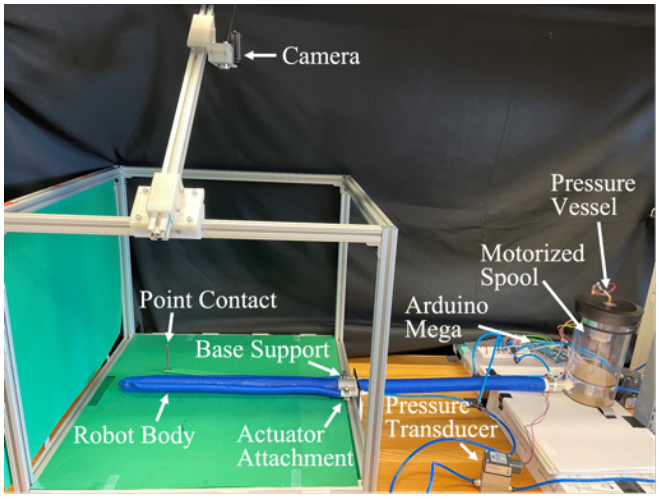

Fig. 4: The experimental setup includes the growing robot and associated control hardware, along with the workspace into which it extends.

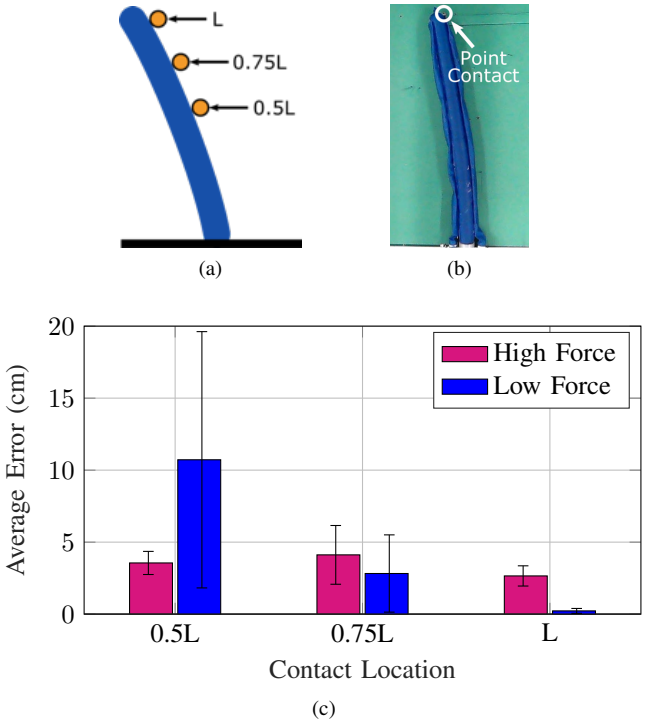

Fig. 5: (a) Schematic illustrating the locations at which point contact forces are applied to the robot body. (b) An image of a low magnitude force applied to the growing robot at location $x = L$. (c) Contact position localization errors after optimization. The mean localization error is 3.44 ± 1.38 cm and 4.59 ± 6.78 cm for high and low magnitude forces, respectively.

C. Two Point Discrimination

In the case where the growing robot is subjected to two contact forces from opposite sides, we seek to determine the distance that the forces must be separated in order to discriminate between them. To determine this distance empirically, we apply one distal contact at the tip of the robot and a second proximal contact at 6 different locations (see Fig. 7a), moving incrementally closer to the distal contact (39 cm, 34 cm, 29 cm, 23.5 cm, 18.5 cm, and 13 cm apart). Again, we apply 0.49 psi to the main robot body and collect image and sensor data 5 times for each loading condition. An example image is shown in Fig. 7b, where the proximal contact is located 29 cm away from the distal contact.

Results in Fig. 7c indicate that when the point contacts are separated by a distance of 23.5 cm or greater (slightly more than two sensor pouch lengths), our proposed optimization approach can effectively determine the location of both points with an average error of 4.49 ± 2.79 cm. Below this threshold however, localization error is much higher, 16.94 ± 2.55 cm on average, suggesting that this is the minimum distance at which our method can effectively discriminate between applied point contacts. As the distance between point forces, which are applied in opposite

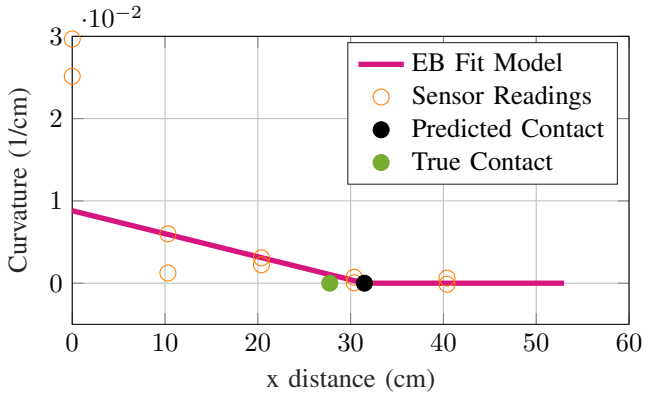

(a)

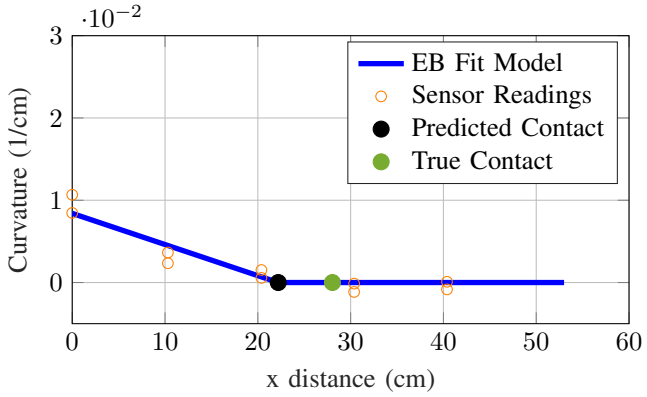

(b)

Fig. 6: Representative example of the optimization results for (a) a high magnitude force and (b) a low magnitude force applied to the growing robot at $x = \frac{L}{2}$. Note the poor estimate of the point contact location in (b) due to the optimization over-fitting to noise in the sensors located on the more proximal half of the robot.

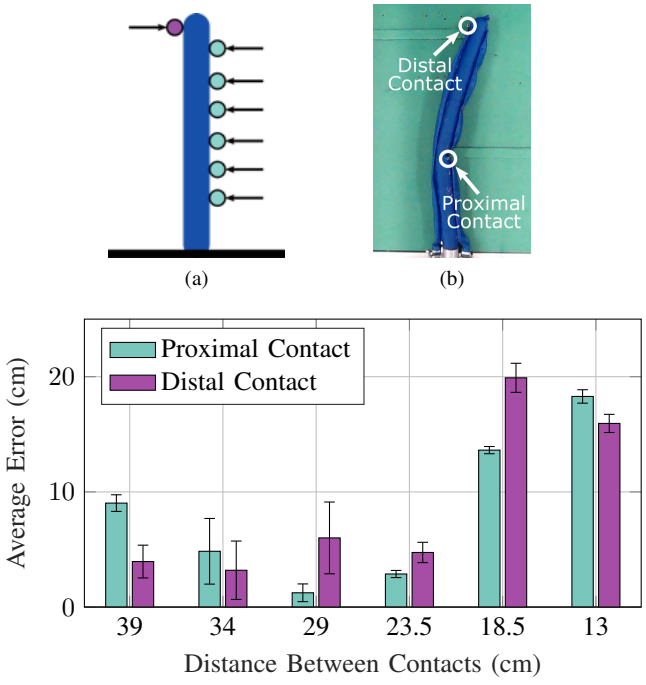

(a) (b) (c)

Fig. 7: (a) Schematic illustrating the locations where point contacts are applied to the robot body. A distal contact (in purple) is held constant at the tip for all cases, while an opposing proximal contact is moved incrementally closer to the distal contact location. (b) An image of the robot when the proximal contact is 29 cm away from the distal contact. (c) Contact force localization errors after optimization.

directions, decreases, the effect each force has on the overall robot shape begins to cancel out that of the other force. This phenomenon leads to smaller measured changes in curvature and increases the impact of sensor noise on the optimization result.

D. Single Contact with Active Bending

Here we consider contact localization for a single contact, similar to Section V-B, but this time for an actuated robot. When an fPAM is actuated, its length decreases, causing the robot body to wrinkle where it is attached to the actuator in order to accommodate this length change and leading to bending of the robot body. While this approach is an effective means of actuation, the significant wrinkling of the material of the robot body induces hard-to-model responses in the sensors attached to an activated actuator. Therefore, for contact localization with actuated growing robots, we only use measurements from the curvature sensors attached to the currently inactive actuator, which is on the outer edge of the curved robot. One full side of sensors is still sufficient to generate an estimate of the robot body shape.

As in Section V-B, we consider contacts occurring at 3 different locations along the robot body at 2 different force magnitudes. We now use the robot's own actuation to initiate contact with the obstacle, as would be the case when the robot is exploring a static, unknown environment, as shown in Fig. 8a. Obstacle locations are chosen such that they are barely touching the robot body at the $\frac{1}{2}L$, $\frac{3}{4}L$, and L lengths when the fPAM actuator pressure is set to 6 psi. For the low and high magnitude force loading cases, we set the actuator pressure to 10 psi and 14 psi respectively. Again, we apply 0.49 psi to the main body of the robot and collect data from 5 trials for each of the 6 loading conditions, the results of which are shown in Fig. 8c.

First, it is important to note that our optimization routine localizes the point contact with low error for all applied locations in the high magnitude force case. The average localization error for these trials is 4.62 ± 0.95 cm (slightly less than the diameter of the actuated robot), which is only slightly higher than it was for the unactuated case. The slight increase in error is to be expected for the actuated case because the localization algorithm only uses measurements from sensors attached to the inactive actuator, making it more susceptible to noisy measurements from any one sensor. For the low magnitude force case, however, the average

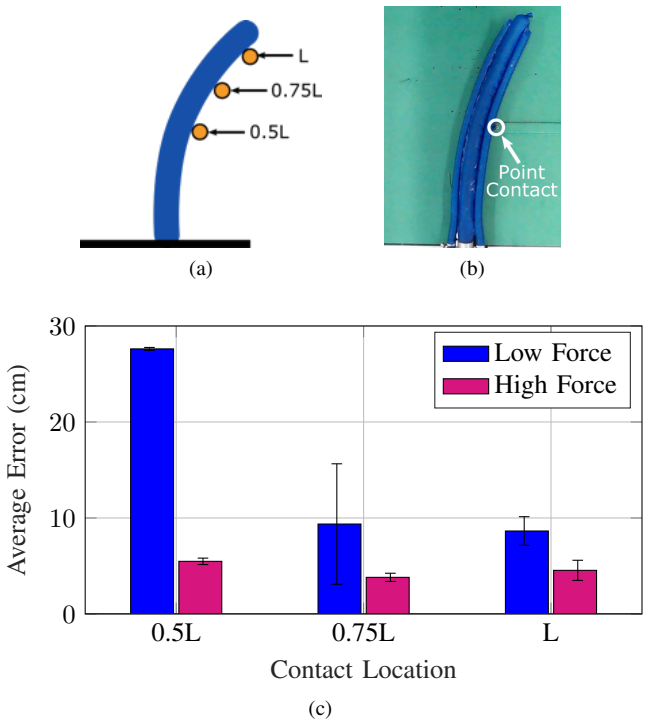

Fig. 8: (a) Schematic illustrating the locations at which the robot collided with point contacts during active bending. (b) An image of a low force collision that occurs at location $x = \frac{L}{2}$. (c) Contact position localization errors after optimization. The mean localization error is 4.62 ± 0.95 cm and 15.21 ± 9.72 cm for the high and low magnitude forces, respectively.

error across all trials, 15.21 ± 9.72 cm, is much higher than the error for high magnitude forces. This large error indicates that the optimization fails to effectively determine the location of the point contact at low forces, likely due to the low magnitude signals failing to overcome the noisy readings from the sensors, and we note that all errors for actuated contact at low forces are higher than the maximum error from the unactuated case (Section V-B). Therefore, in order to determine the location of smaller forces on an actuated growing robot, more sensor measurements are necessary.

E. Single Contact with Active Bending and Growing

Finally, we consider a scenario where a growing robot is exploring an unknown environment. We make use of tactile perception to determine when and where an obstacle is in contact with the robot. Such information could be valuable for use in a planning algorithm (e.g. [8]) or to identify a support structure the robot could anchor itself to, as proposed in [20].

We place the unknown obstacle for the robot to encounter at the same location as that of the furthest obstacle used in Section V-D. This location is chosen because we have found that using fewer than 5 sensor measurements — which is the number of available measurements when our current robot is actuated and fully everted — for optimization, leads to less reliable localization. We discuss this current limitation of our method and robot hardware, along with future approaches that can address this challenge, in Section VI.

In order to explore the workspace, the robot first grows one sensor length and then executes a sweeping motion generated by sending a sine wave to the fPAM actuators with an amplitude equal to the maximum pressure the actuator can reliably hold (18 psi). If a contact is detected during the sweeping motion (as described in Section IV), we average 10 sensor measurements recorded at the peak of the sine wave to use to localize the contact. We choose to use the sensor readings collected when the actuator is at maximum pressure based on the results of Section V-D, which show consistently lower point contact localization errors for higher forces applied to the obstacle. To achieve robot growth, we use the minimum possible body pressure at all times, which keeps the bending stiffness of the robot low and allows it to achieve higher curvature configurations. For growth lengths from zero to $\frac{L}{2}$, growth is achieved with a pressure of 1.47 psi. For lengths $\frac{L}{2}$ to $\frac{2L}{3}$ we apply 1.01 psi, and from $\frac{2L}{3}$ to L we apply 0.49 psi. Pressure to curvature mappings are created for each body pressure following the same method detailed in Section II-B.

Results of the experiment are shown in Fig. 9. Our method successfully identifies when the robot is in contact with an obstacle and localizes the contact with 6.82 cm error. It is worthwhile to note that this error is higher than the average of the previous experiment in Section V-D. This increased error is likely due to additional noise in the sensor readings caused by the rapid change in curvature of the eversion process that facilitates robot growth. When the sensors are in a straight configuration, as they are immediately after robot growth, they should measure zero curvature. In reality, however, we find that there is a delay in the sensor response as it goes from a highly bent configuration to a straighter configuration, which contributes to the increased localization error. In future, this delay could be modeled and compensated for so as to mitigate its impact on the optimization.

VI. Discussion and Conclusion

In this work, we have presented an approach to enable tactile sensing for growing robots. Our approach consists of a method to integrate flexible, off-the-shelf sensors into the body of a growing robot via a pouch design, along with an optimization routine to deduce the locations of point contacts on the robot body based on these sensor measurements. We experimentally characterized the error of this approach in localizing a single contact applied to both an actuated and unactuated robot and determined a threshold beyond which it was possible to distinguish between two separate contact forces applied to the unactuated robot. Finally, we showed that this method was able to detect and localize an obstacle that came into contact with a growing robot as it explored unknown surroundings.

It is important to note a few limitations of the current approach. In particular, the performance of our proposed

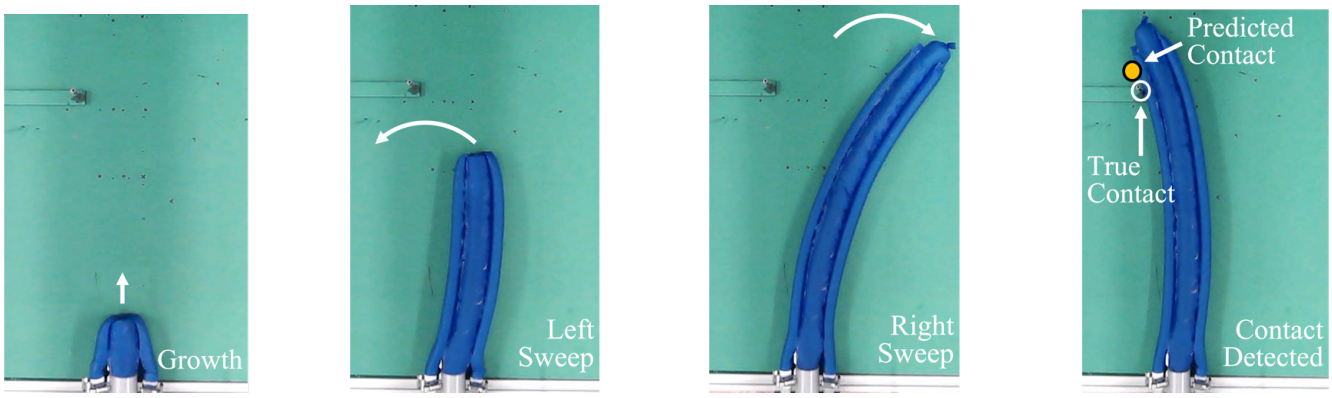

(a) (b) (c) (d)

Fig. 9: (a)-(c) Images of the robot growing and bending over time, exploring an environment containing an obstacle with unknown location. (d) The robot collides with the unknown obstacle, triggering the localization algorithm, which returns an estimate of the location of the contact force applied to the robot. The error between the predicted point contact and actual point contact is 6.82 cm.

method for tactile sensing decreases considerably when only a few sensor measurements (fewer than 5) are available, due to noise corrupting each sensor measurement. Extending the current optimization framework to take into account statistics of the noise associated with each sensor, could help improve localization robustness. Additionally, as soft sensing technology continues to develop, other types of curvature sensors with better signal to noise ratios can be investigated for use with the proposed method. Overall, we believe that our method for tactile perception in growing robots can be used either on its own, or in conjunction with other sensing devices — such as the tip-mounted camera in [3] — to enable better mapping and autonomous exploration algorithms for unknown environments.

REFERENCES

[1] E. W. Hawkes, L. H. Blumenschein, J. D. Greer, and A. M. Okamura, "A soft robot that navigates its environment through growth," *Science Robotics*, vol. 2, no. 8, 2017.

[2] P. A. der Maur, B. Djambazi, Y. Haberthür, P. Hörmann, A. Kübler, M. Lustenberger, S. Sigrist, O. Vigen, J. Förster, F. Achermann *et al.*, "Roboa: Construction and evaluation of a steerable vine robot for search and rescue applications," in *2021 IEEE 4th International Conference on Soft Robotics (RoboSoft)*, 2021, pp. 15–20.

[3] M. M. Coad, L. H. Blumenschein, S. Cutler, J. A. Reyna Zepeda, N. D. Naclerio, H. El-Hussieny, U. Mehmood, J.-H. Ryu, E. W. Hawkes, and A. M. Okamura, "Vine robots: Design, teleoperation, and deployment for navigation and exploration," *IEEE Robotics Automation Magazine*, vol. 27, no. 3, pp. 120–132, 2020.

[4] J. Luong, P. Glick, A. Ong, M. S. deVries, S. Sandin, E. W. Hawkes, and M. T. Tolley, "Eversion and retraction of a soft robot towards the exploration of coral reefs," in *IEEE Int. Conf. on Soft Robotics*, April 2019, pp. 801–807.

[5] M. Li, R. Obregon, J. J. Heit, A. Norbash, E. W. Hawkes, and T. K. Morimoto, "Vine catheter for endovascular surgery," *IEEE Transactions on Medical Robotics and Bionics*, vol. 3, no. 2, pp. 384–391, 2021.

[6] D. A. Haggerty, N. D. Naclerio, and E. W. Hawkes, "Characterizing environmental interactions for soft growing robots," in *2019 IEEE/RSJ International Conference on Intelligent Robots and Systems (IROS)*, 2019, pp. 3335–3342.

[7] J. D. Greer, L. H. Blumenschein, A. M. Okamura, and E. W. Hawkes, "Obstacle-aided navigation of a soft growing robot," in *2018 IEEE International Conference on Robotics and Automation (ICRA)*, 2018, pp. 4165–4172.

[8] M. Selvaggio, L. Ramirez, N. D. Naclerio, B. Siciliano, and E. W. Hawkes, "An obstacle-interaction planning method for navigation of actuated vine robots," in *2020 IEEE International Conference on Robotics and Automation (ICRA)*, 2020, pp. 3227–3233.

[9] C. Watson, R. Obregon, and T. K. Morimoto, "Closed-loop position control for growing robots via online jacobian corrections," *IEEE Robotics and Automation Letters*, vol. 6, no. 4, pp. 6820–6827, 2021.

[10] J. D. Greer, T. K. Morimoto, A. M. Okamura, and E. W. Hawkes, "A soft, steerable continuum robot that grows via tip extension," *Soft robotics*, vol. 6, no. 1, pp. 95–108, 2019.

[11] C. Watson and T. K. Morimoto, "Permanent magnet-based localization for growing robots in medical applications," *IEEE Robotics and Automation Letters*, vol. 5, no. 2, pp. 2666–2673, 2020.

[12] S.-G. Jeong, M. M. Coad, L. H. Blumenschein, M. Luo, U. Mehmood, J. H. Kim, A. M. Okamura, and J.-H. Ryu, "A tip mount for transporting sensors and tools using soft growing robots," in *2020 IEEE/RSJ International Conference on Intelligent Robots and Systems (IROS)*, 2020, pp. 8781–8788.

[13] A. M. Gruebele, A. C. Zerbe, M. M. Coad, A. M. Okamura, and M. R. Cutkosky, "Distributed sensor networks deployed using soft growing robots," in *2021 IEEE 4th International Conference on Soft Robotics (RoboSoft)*, 2021, pp. 66–73.

[14] V. A. Aloi and D. C. Rucker, "Estimating loads along elastic rods," in *2019 International Conference on Robotics and Automation (ICRA)*, 2019, pp. 2867–2873.

[15] Y. Chen, L. Wang, K. Galloway, I. Godage, N. Simaan, and E. Barth, "Modal-based kinematics and contact detection of soft robots," *Soft Robotics*, vol. 8, no. 3, pp. 298–308, 2021.

[16] J. Braam, "In touch: plant responses to mechanical stimuli," *New Phytologist*, vol. 165, no. 2, pp. 373–389, 2005.

[17] W. Fichter, *A theory for inflated thin-wall cylindrical beams*. National Aeronautics and Space Administration, 1966, vol. 3466.

[18] N. D. Naclerio and E. W. Hawkes, "Simple, low-hysteresis, foldable, fabric pneumatic artificial muscle," *IEEE Robotics and Automation Letters*, vol. 5, no. 2, pp. 3406–3413, 2020.

[19] S. Bektas and Y. Sisman, "The comparison of l1 and l2-norm minimization methods," *International Journal of the Physical Sciences*, vol. 5, no. 11, pp. 1721–1727, 2010.

[20] M. Wooten, C. Frazelle, I. D. Walker, A. Kapadia, and J. H. Lee, "Exploration and inspection with vine-inspired continuum robots," in *2018 IEEE International Conference on Robotics and Automation (ICRA)*, 2018, pp. 5526–5533.